Journal of Sound and Vibration 329 (2010) 1601–1614

Contents lists available at ScienceDirect

Journal of Sound and Vibration

journal homepage: www.elsevier.com/locate/jsvi

Active vibration isolation of a system with a distributed parameter isolator using absolute velocity feedback control

B. Yan, M.J. Brennan *, S.J. Elliott, N.S. Ferguson

Institute of Sound and Vibration Research, University of Southampton, Southampton SO17 1BJ, UK

ARTICLE INFO

Article history:
Received 23 February 2009
Received in revised form
8 November 2009
Accepted 17 November 2009
Handling Editor: J. Lam
Available online 22 December 2009

ABSTRACT

This paper is concerned with the active isolation of a system containing a distributed parameter isolator using absolute velocity feedback control. The main differences between this type of system and one with a massless isolator, is that there are isolator resonances. It is shown that the vibration at these resonance frequencies cannot be suppressed using a simple velocity feedback control strategy. Moreover, it is found that the isolator resonances can cause the control system to become unstable, if the isolated equipment is supported on a flexible base. A stability criterion based on the mode shapes of the system is presented. Two techniques to stabilise the system are investigated and compared. The first involves the addition of mass on the base structure, and the second involves an electronic lead compensator. Experimental results are presented to support the theoretical findings. It is shown that even if the instability due to the isolator resonances and flexibility of the base can be prevented, the instability due to the flexibility of the equipment remains a problem.

1. Introduction

Among the various issues associated with vibration, the isolation of a delicate item of equipment from a vibrating host structure is a common situation [1–3]. Traditionally, passive vibration isolation, consisting of vibration isolators made of compliant materials, is often used to provide dynamic decoupling between the delicate equipment and the host structure [2]. Base vibration typically has an unpredictable waveform and the vibration isolator has to deal with broadband excitation spectra [4]. Conventional passive vibration isolation systems suffer from an inherent trade-off in the choice of damping for high frequency isolation, which requires a low level of damping, and isolation at the fundamental mounted resonance frequency, which requires a high level of damping [4,5]. This inherent compromise can be overcome by incorporating an active vibration isolation system in parallel with a passive isolator [4,6–8].

In active vibration isolation, the output of the system can be fed back into the controller directly to generate the control signal, which is simple and straightforward to implement. A common approach is to use absolute velocity feedback (AVF) control [9–11]. One of the advantages of this approach is that the control system is unconditionally stable for collocated ideal force actuators and sensors, irrespective of structural modelling errors [9,12]. Furthermore, AVF control is the optimal solution to minimise the mean square velocity of the equipment [8]. For a base-excited system, the action of AVF control is equivalent to a skyhook damper [6]; the response at the resonance frequency is attenuated without compromising high frequency performance. If the base is rigid, the control system is unconditionally stable [13].

* Corresponding author.
E-mail address: mjb@isvr.soton.ac.uk (M.J. Brennan).

0022-460X/$ - see front matter © 2009 Elsevier Ltd. All rights reserved.
doi:10.1016/j.jsv.2009.11.023

The traditional active vibration isolation model, in which the mass of the isolator is ignored, offers a good prediction tool and provides design guidelines at relatively low frequencies. However, at higher frequencies, the predictions based on the massless isolator model may be wrong and misleading. The distributed mass, stiffness and damping in the isolator introduce isolator resonances (IRs), or wave effects, in the isolator [14–16]. The degradation in passive performance of the vibration isolator due to the isolator resonances is especially important for lightly damped metallic isolators, since the smaller the damping in the isolator the more significant are the resonances caused by the wave effects [17].

The aim of this paper is to investigate the effects of resonances in a distributed parameter isolator on the control performance and stability of an active vibration isolation system under AVF control. A base-excited SDOF system with a distributed parameter isolator, which is modelled as a finite elastic rod, is first analysed under AVF control. This analysis is then extended to include the resonance behaviour of the supporting structure. The control performance and stability of such systems are discussed. Experimental work on a four-spring active vibration isolation system is then presented to support and validate the theoretical results before the overall conclusions are drawn.

2. Active vibration isolation of the system under base-excitation

The base-excited active vibration isolation system considered in this section is shown in Fig. 1a. It consists of an item of equipment represented by its impedance Z_e supported by a distributed parameter isolator under AVF control. The isolator

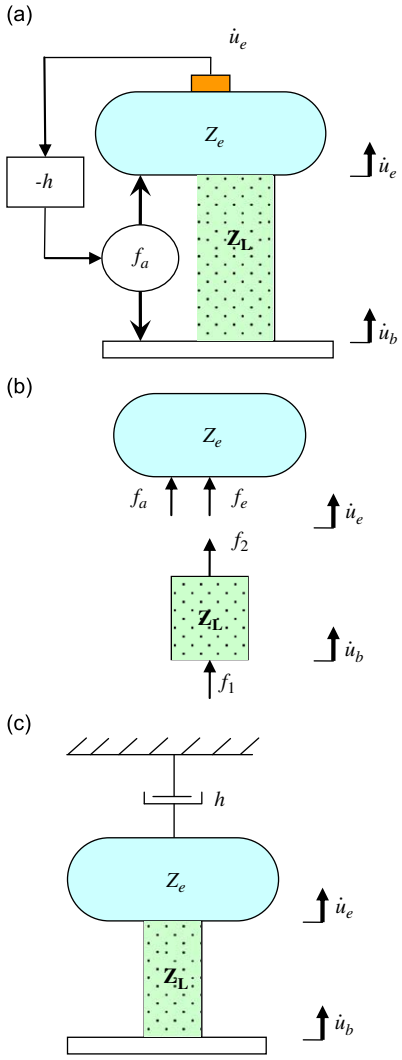

Fig. 1. Active isolation of a base-excited system, in which the isolator is a distributed parameter system: (a) schematic diagram, (b) free-body diagram, and (c) passive analogue of the active control system.

is modelled as an elastic rod, and connects to the equipment at a single point. Its impedance matrix is given by [17]

$$\mathbf{Z_L} = \begin{bmatrix} Z_{11} & Z_{12} \\ Z_{21} & Z_{22} \end{bmatrix} = \frac{S\sqrt{E^*\rho}}{\mathrm{j}\sin(k_l^* L)} \begin{bmatrix} \cos(k_l^* L) & -1 \\ -1 & \cos(k_l^* L) \end{bmatrix} \tag{1}$$

where L, S, E^* and ρ are the length, cross-sectional area, Young's modulus and density of the isolator, respectively. To account for damping in the isolator, Young's modulus is assumed to be complex, i.e. $E^* = E(1+\mathrm{j}\eta_i)$, where η_i is the loss factor of the isolator. The complex longitudinal wavenumber k_l^*, is given by $k_l^* \approx k_l(1-\mathrm{j}\eta_i/2)$, where $k_l = \sqrt{\rho/E}\omega$, and ω is angular frequency. The active control force, f_a, acts in parallel with the isolator between the equipment and the base. The control force is proportional to, and in phase with, the velocity of the equipment, and the feedback controller has a constant gain $-h$. Thus

$$f_a = -h\dot{u}_e \tag{2}$$

The free-body diagram of the active isolation system is shown in Fig. 1b, and the system of equations describing the system is

$$Z_e\dot{u}_e = f_a + f_e \tag{3a}$$

$$\begin{bmatrix} f_1 \\ f_2 \end{bmatrix} = \mathbf{Z_L} \begin{bmatrix} \dot{u}_b \\ \dot{u}_e \end{bmatrix} \tag{3b}$$

Eqs. (2) and (3) can be combined to give the transmissibility of the system, which is given by

$$T = \frac{\dot{u}_e}{\dot{u}_b} = \frac{-Z_{21}}{Z_e + Z_{22} + h} \tag{4}$$

If the equipment is modelled as a mass, i.e. $Z_e = \mathrm{j}\omega m_e$, and the elements of impedance matrix given in Eq. (1) substituted into Eq. (4), the transmissibility can be written in non-dimensional form as

$$T = \frac{1}{\cos\left[\sqrt{\mu_i}\left(1-\mathrm{j}\frac{\eta_i}{2}\right)\Omega\right] - \frac{\Omega - \mathrm{j}2\zeta_a}{\sqrt{\mu_i}}\left(1-\mathrm{j}\frac{\eta_i}{2}\right)\sin\left[\sqrt{\mu_i}\left(1-\mathrm{j}\frac{\eta_i}{2}\right)\Omega\right]} \tag{5}$$

where $\Omega = \omega/\omega_e$ is the ratio of the excitation frequency ω, to the system fundamental natural frequency $\omega_e = \sqrt{K_L/m_e}$ (note that the mass of the isolator is neglected in the definition of OMEGA), due to the interaction of the equipment mass and the static stiffness, $K_L = ES/L$, of the isolator; $\mu_i = \rho SL/m_e$ is the ratio of the mass of the isolator to the mass of the equipment and $\zeta_a = h/2\sqrt{K_L m_e}$ is the active damping ratio due to AVF control.

Examining Eq. (5) it can be seen that the effect of AVF control is to add a damping term to the denominator, leaving the numerator unchanged. The action of AVF control in this case is therefore the same as a skyhook damper. Note that the equivalent viscous damper acting between the equipment and the inertial ground has a damping coefficient h. The transmissibility is plotted in Fig. 2 for various active damping ratios, and for $\mu_i = 0.1$ and $\eta_i = 0.01$. Also plotted is the transmissibility of a system with a massless isolator. It can be seen that the fundamental peak in the transmissibility for the distributed parameter isolator occurs at a frequency close to that of the resonance frequency of the system with a

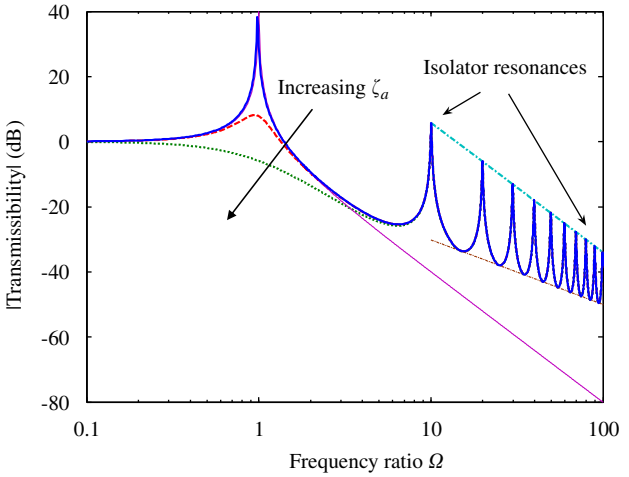

Fig. 2. Transmissibility of the base-excited active vibration isolation system under AVF control. Mass ratio, $\mu_i = 0.1$, isolator loss factor, $\eta_i = 0.01$. The active damping ratios $\zeta_a = 0$, solid bold line; $\zeta_a = 0.2$, dashed line; and $\zeta_a = 1$, dotted line. The thick and thin dashed-dotted lines pass through the isolator resonance peaks and the troughs of the transmissibility respectively. The faint solid line is the transmissibility for the system with a massless isolator, which has no isolator resonances.

massless isolator. However, at high frequencies ($\Omega \gg 1$), the transmissibility for the system with the distributed parameter isolator, is greater than that for the massless isolator, due to the isolator resonances. It can also be seen that the fundamental resonance peak is attenuated when the active damping ratio is increased, but there is little reduction of the peaks of the isolator resonances. Two other lines are also plotted: one which passes through the isolator resonance peaks and one which passes through the troughs. Approximate expressions for these lines are determined below.

To determine the line which passes through the peaks, it is first noted that these peaks occur approximately at a natural frequency of the isolator when $\sin(\sqrt{\mu_i}\Omega)=0$. By making small angle approximations, but assuming that $\Omega \gg \zeta_a$, i.e., relatively high frequencies, then the line that passes through the peaks is given by

$$|T|_{\text{peak}} \approx \frac{2}{\eta_i}\frac{1}{\Omega^2} \tag{6}$$

This demonstrates that AVF control cannot attenuate the peaks of the isolator resonances in the distributed parameter isolator at high frequencies.

To determine the line through the troughs it is noted that a trough occurs approximately when $\sin(\sqrt{\mu_i}\Omega)=1$ and when $\cos(\sqrt{\mu_i}\Omega)=0$. Again, using small angle approximations and assuming $\Omega \gg \zeta_a$, i.e., relatively high frequencies, the line that passes through the troughs is determined to be

$$|T|_{\text{trough}} \approx \sqrt{\mu_i}\frac{1}{\Omega} \tag{7}$$

which shows that AVF control cannot influence the line though the troughs either. A more general and physical argument to show why AVF control cannot change the transmissibility of the system at high frequencies, can be presented by considering the relative size of the impedances of the system components in Eq. (4). As mentioned previously, the active control system effectively acts as a sky-hook damper with damping coefficient h. This damper acts in parallel with the point impedance of the isolator Z_{22} and the equipment impedance Z_e as can be seen by the denominator of Eq. (4), $Z_e+Z_{22}+h$. At relatively high frequencies, if the equipment has a mass-like impedance, i.e. $Z_e = j\omega m_e$ which increases with frequency, then this impedance is likely to be much higher than the control gain h. It will thus control the response, rendering AVF control ineffective.

Because the controller has a constant feedback gain, the stability of the AVF control system can be determined by examining the plant response rather than the open-loop response function of the system. By combining Eqs. (3a,b), the plant response is given by

$$G = \left.\frac{\dot{u}_e}{f_a}\right|_{\dot{u}_b=0} = \frac{1}{Z_e+Z_{22}} \tag{8}$$

It is noted that Z_e and Z_{22} are both point impedances, so their phase is between -90° and 90°. Therefore the overall phase shift of the plant response G is between -90° and 90°, and is thus completely passive and hence stable. Also, from the point of view of collocation, because the base motion is prescribed which is not affected by the active control force, the actuator and the sensor are thus collocated, so that such a system under AVF control is unconditionally stable.

3. Active vibration isolation of the system on a flexible base

In practice, the base structure is not usually rigid as discussed in the previous section. It typically exhibits dynamic behaviour, and thus the AVF control system is no longer co-located. In this section an investigation is carried out into the way in which the base dynamics affects the control performance and the system stability. Fig. 3a depicts the system under consideration. The base structure is excited by a primary force f, and is represented by its input impedance Z_b. The isolator is again modelled as an elastic rod.

Using the free-body diagram in Fig. 3b, the system can be described by Eqs. (3a, b) and

$$Z_b\dot{u}_b = f - f_a + f_b \tag{9}$$

where $f_b = -f_1$ is an internal force. The velocity of the equipment is thus given by

$$\dot{u}_e = (Y_{ee} - Y_{eb})f_a + Y_{eb}f \tag{10}$$

where Y_{ee} is the input mobility of the equipment when coupled to the rest of the system, Y_{eb} is the transfer mobility from the force, f on the base to the equipment velocity, $\dot{u}_e$ when the system is connected, and they are, respectively, given by

$$Y_{ee} = \frac{Z_b+Z_{11}}{(Z_e+Z_{22})(Z_b+Z_{11}) - Z_{12}Z_{21}} \tag{11a}$$

$$Y_{eb} = \frac{-Z_{21}}{(Z_e+Z_{22})(Z_b+Z_{11}) - Z_{12}Z_{21}} \tag{11b}$$

Substituting Eq. (2) into (10), the velocity of the equipment can be written in terms of the mobilities as

$$\frac{\dot{u}_e}{f} = \frac{Y_{eb}}{1+h(Y_{ee}-Y_{eb})} \tag{12}$$

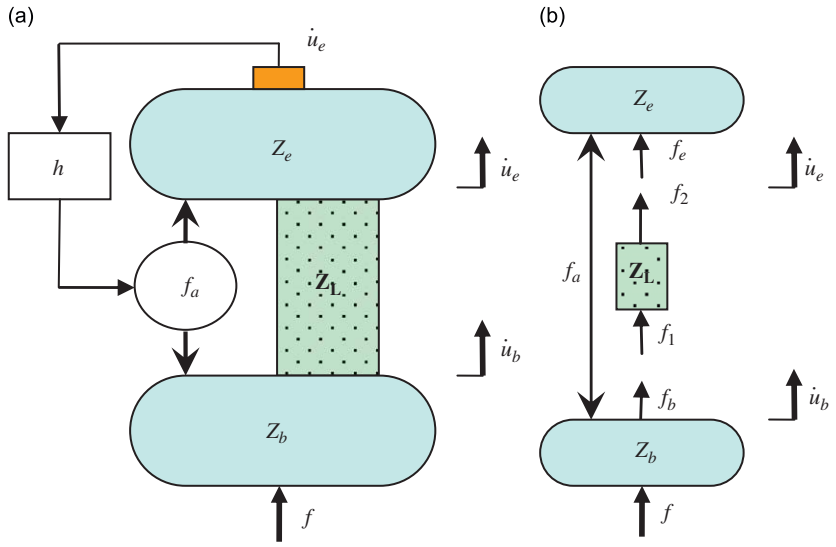

Fig. 3. Active isolation of a system on a flexible base, in which the isolator is a distributed parameter system: (a) schematic diagram, and (b) free-body diagram.

If the equipment has a mass-like impedance, i.e. $Z_e = \mathrm{j}\omega m_e$ and the base structure is modelled as a mass m_b on a complex spring, i.e. $K_b^* = K_b(1+\mathrm{j}\eta_b)$, where K_b is the stiffness of the base and η_b is the loss factor of the base, the non-dimensional amplitude ratio of the system under AVF control is given by

$$\frac{u_e}{\delta_{st}} = \frac{1}{\left[\left[(1+\mathrm{j}\eta_b)-\left(1+\frac{1}{\mu_b}\right)\frac{\Omega^2}{\Gamma^2}\right]\cos\left[\sqrt{\mu_i}(1-\mathrm{j}\frac{\eta_i}{2})\Omega\right]-\left[(1+\mathrm{j}\eta_b)+\mu_k\mu_i(1+\mathrm{j}\eta_i)-\frac{\Omega^2}{\Gamma^2}\right]\frac{\Omega}{\sqrt{\mu_i}}(1-\mathrm{j}\frac{\eta_i}{2})\sin\left[\sqrt{\mu_i}(1-\mathrm{j}\frac{\eta_i}{2})\Omega\right]\right.$$
$$\left.+\mathrm{j}2\zeta_a\left\{\mu_k\Omega\left[\cos\left(\sqrt{\mu_i}\left(1-\mathrm{j}\frac{\eta_i}{2}\right)\Omega\right)-1\right]+\frac{1}{\sqrt{\mu_i}}\left(1-\mathrm{j}\frac{\eta_i}{2}\right)\left(1+\mathrm{j}\eta_b-\frac{\Omega^2}{\Gamma^2}\right)\sin\left(\sqrt{\mu_i}\left(1-\mathrm{j}\frac{\eta_i}{2}\right)\Omega\right)\right\}\right] \quad (13)$$

where $\delta_{st} = f/K_b$ is the static deflection of the base; $\Gamma = \omega_b/\omega_e = 1/\sqrt{\mu_k\mu_b}$ is the ratio of the natural frequency of the base to the natural frequency of the equipment, in which $\omega_b = \sqrt{K_b/m_b}$ (note that the mass of the isolator is neglected in the definition of GAMMA); $\mu_k = K_L/K_b$ is the ratio of the static stiffness of the isolator to the stiffness of the base; $\mu_b = m_b/m_e$ is the ratio of the mass of the base to the mass of the equipment.

It can be seen in Eq. (13) that, as before, the effect of AVF control is to add a damping term to the denominator and leave the numerator unchanged. The amplitude ratio for the system on a flexible base under AVF control with different values of the active damping ratio ζ_a, is plotted in Fig. 4. It can be seen that the fundamental resonance peak is attenuated with an increase in the active damping ratio. The peak that is primarily due to the base dynamics, which is the second peak, is also reduced for high active damping ratios. However, the peaks of the isolator resonances are largely unaffected by the control system, especially at high frequencies. The reason is the same as that discussed for the base excited system. However, it should be noted that some isolator resonance peaks, such as the third peak, are amplified due to AVF control. This amplification can potentially destabilise the control system at high control gains, and thus the control performance is limited.

The stability of the control system can also be determined by examining the plant response. From Eq. (10), the plant response is given by

$$G = \left.\frac{\dot{u}_e}{f_a}\right|_{f=0} = Y_{ee} - Y_{eb} \quad (14)$$

Because Y_{ee} is an input mobility, it has a phase shift between -90° and 90°. However, Y_{eb} is a transfer mobility so it is a potential threat to the stability of the AVF control system. Moreover, if the AVF control system is only conditionally stable, there is at least one loop in the left half in the Nyquist plot of the plant response which crosses the negative real axis. For the system analysed here, these loops only occur at resonance frequencies. Thus, if the transfer mobility Y_{eb} is greater than the input mobility Y_{ee} at one of the resonance frequencies, the system has the potential to become unstable for high control gains. Based on this fact a stability condition for the control system can be derived.

For a multi-degree-of freedom system, the mobility is given by [5]

$$Y_{ts} = \frac{\dot{u}_t}{f_s} = \sum_{j=1}^{\infty}\frac{\mathrm{j}\omega\cdot\phi_t^{(j)}\cdot\phi_s^{(j)}}{K_j(1-\Omega_j^2+\mathrm{j}2\zeta_j\Omega_j)} \quad (15)$$

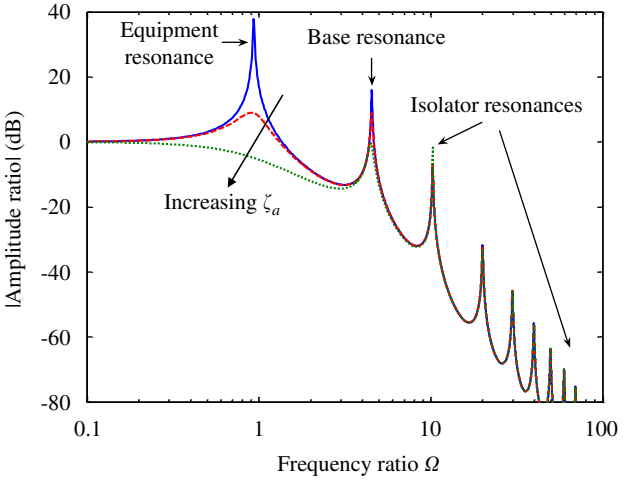

Fig. 4. Amplitude ratio of the active vibration isolation system with parameters $\mu_i = 0.1$, $\eta_i = 0.01$, $\mu_b = 0.5$, $\mu_k = 0.1$, $\eta_b = 0.01$, containing a distributed parameter isolator on a flexible base under AVF control. The active damping ratios are $\zeta_a = 0$, solid line; $\zeta_a = 0.2$, dashed line; and $\zeta_a = 1$, dotted line.

where $\phi_t^{(j)}$ and $\phi_s^{(j)}$ is the jth mode shape evaluated at the response point t and excitation point s, respectively; K_j, M_j and ζ_j are the modal stiffness, modal mass and equivalent modal viscous damping ratio of the jth mode, respectively; $\Omega_j = \omega/\omega_j$ is the non-dimensional frequency ratio, where $\omega_j = \sqrt{K_j/M_j}$. In a lightly damped multi-degree-of-freedom system only one mode dominates at frequencies close to a natural frequency, and in this case the point and transfer mobilities can be approximated to

$$Y_{ee} \approx \frac{[\phi_e^{(j)}]^2}{2\sqrt{K_j M_j}\zeta_j}, \tag{16a}$$

$$Y_{eb} \approx \frac{(\phi_b^{(j)}\phi_e^{(j)})}{2\sqrt{K_j M_j}\zeta_j} \tag{16b}$$

where $\phi_e^{(j)}$ and $\phi_b^{(j)}$ are the jth mode shape evaluated at the equipment and base respectively. Substituting Eqs. (16a, 16b) into (14), the plant response at a natural frequency can be written as

$$G|_{\omega \approx \omega_j} \approx \frac{[\phi_e^{(j)}]^2\left(1 - \dfrac{\phi_b^{(j)}}{\phi_e^{(j)}}\right)}{2\sqrt{K_j M_j}\zeta_j} \tag{17}$$

For stability, the following condition is necessary

$$\frac{\phi_b^{(j)}}{\phi_e^{(j)}} < 1 \tag{18}$$

for all j. If the mode shapes of the system, evaluated at the equipment and base, have the same phase, then the condition for stability is $|\phi_e^{(j)}| > |\phi_b^{(j)}|$. Thus Eq. (18) provides a simple method to determine the stability of the AVF control system in terms of the mode shapes of the system. This stability condition means that if the displacement of the base is greater than the displacement of the equipment, and these two displacements are in phase at the jth natural frequency, the AVF control system may become unstable. This stability condition can also be applied to the AVF control system containing a massless isolator on a flexible base, which has been previously investigated by Elliott et al. [13].

Figs. 5(a)–(c), depict the plant frequency response (magnitude, phase and zoomed (0–100 Hz) Nyquist plot) for a conditionally stable AVF control system. It can be seen in Fig. 5(b) that the phase at the first isolator resonance frequency is $< -180^\circ$. This phase lag generates a loop in the left half of the complex plane as shown in Fig. 5(c) that crosses the negative real axis, which causes the system to be potentially unstable for high control gains.

To stabilise the control system, the stability condition given in Eq. (18), shows that the relative displacement between the equipment and the base at a troublesome resonance frequency needs to be adjusted. In some situations, this can simply be achieved by adding more damping in the isolator. Additional mass could also be added to the base structure to change the mode shape [18]. Alternatively, electronic means such as lead compensators can be used to compensate for the phase

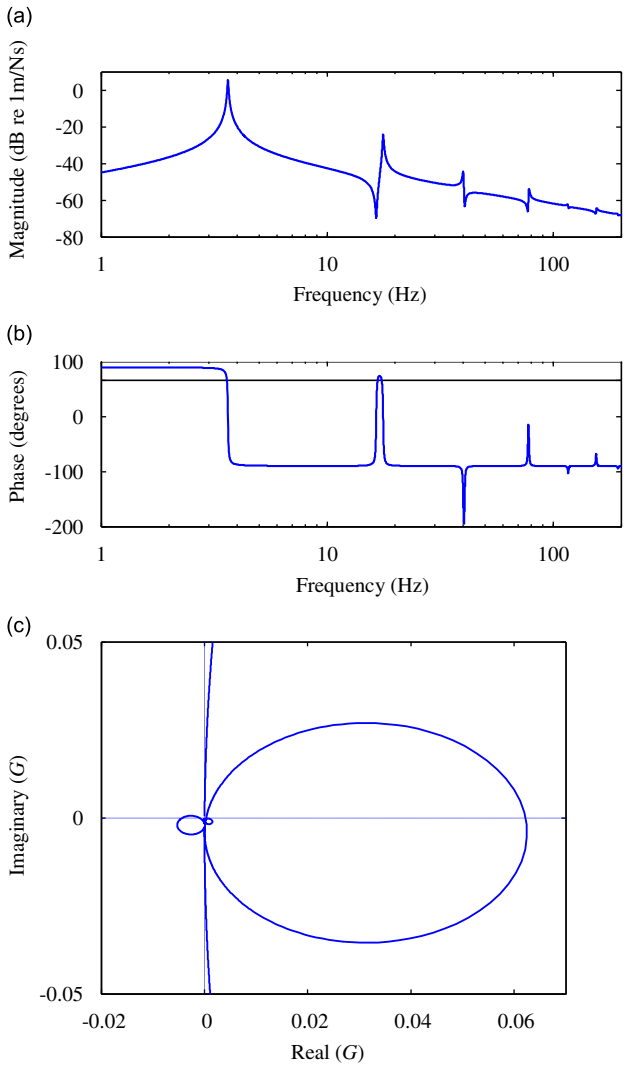

Fig. 5. Plant frequency response: (a) magnitude, (b) phase, and (c) Nyquist plot (0–1000 Hz). $\mu_i = 0.1$, $\mu_b = 0.5$, $\mu_k = 0.1$, $\eta_i = \eta_b = 0.01$.

lag at troublesome resonance frequency. To guarantee stability, at a resonance frequency it is necessary for

$$hG = h\frac{[\phi_e^{(j)}]^2\left(1-\dfrac{\phi_b^{(j)}}{\phi_e^{(j)}}\right)}{2\sqrt{K_jM_j}\zeta_j} > -1 \tag{19}$$

Hence the maximum control gain is given by

$$h_{\max} = \frac{2\sqrt{K_jM_j}\zeta_j}{[\phi_e^{(j)}]^2\left(\dfrac{\phi_b^{(j)}}{\phi_e^{(j)}}-1\right)} \tag{20}$$

4. Experimental investigation

4.1. Experimental setup

To investigate some of the theoretical findings in the previous section an experimental investigation was carried out. In the theoretical analysis, the distributed parameter isolator was modelled as an elastic rod. In the experimental work, a helical spring was used. For practical reasons a four-spring active vibration isolation system was designed rather than a single spring system, and a photograph of this is shown in Fig. 6. It consisted of a symmetrical aluminium plate

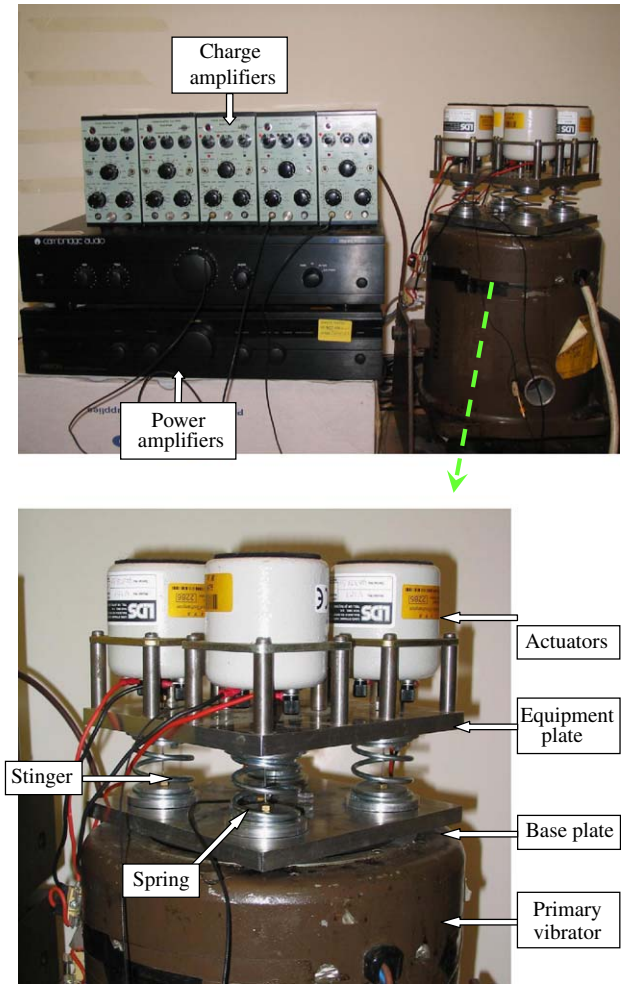

Fig. 6. Photographs of the four-spring active vibration isolation system.

representing the equipment installed on top of another symmetrical aluminium plate representing the base via four identical helical springs. A large electromagnetic vibrator (Derritron type VP4) beneath the base plate acted as the primary force actuator, and the four small electromagnetic actuators (LDS V101) fixed on the equipment plate were the control actuators at each mount position. The equipment structure to be isolated was thus a combination of the aluminium equipment plate and four actuators. Each helical spring was bolted to the equipment plate through an aluminium washer beneath each actuator. A stinger was connected through the centre of the spring between each actuator and the corresponding washer at the foot of each spring. The base plate, to which the washers were attached by bees wax, was bolted to the primary vibrator with four bolts. The base structure can be modelled as a SDOF system as it is symmetric, i.e. a flexible base with an effective mass supported by a spring. Therefore, this four-spring active vibration isolation system can be simulated using the theoretical model described in the previous section. The detailed physical and geometrical parameters of the experimental setup are listed in Table 1. A schematic diagram of the experimental setup and signal path with details of one actuator and the corresponding spring is shown in Fig. 7.

4.2. Stability analysis

To measure the open-loop frequency response, the four actuators fixed on top of the equipment plate were driven with the same white noise from a dynamic signal analyser (Data Physics-Signalcalc Mobilyzer II) through a power amplifier, while the primary vibrator was connected but inactive. The equipment response was measured using five accelerometers (B&K type 4375) located along two central lines of the equipment plate, and the signals passed through charge amplifiers (B&K type 2635) and integrated, so that the vertical equipment velocity response could be measured. The open-loop frequency response of the AVF control system was thus obtained, but the input voltage to the power amplifier was used as

Table 1
Physical properties and geometrical data of the four-spring active vibration isolation system.

Equipment structure	Material of the equipment plate	Aluminum
	Dimension of the equipment plate	$(160 \times 160 \times 10\,\text{mm})$
	Mass of each actuator	0.91 kg
	Mass of the equipment structure	5 kg
Spring	Mass of each spring	27.1 g
	Stiffness of each spring	1.73×10^4 N/m
Base structure	Material of the base plate	Aluminum
	Dimension of the base plate	$(160 \times 160 \times 10\,\text{mm})$
	Effective mass	1.18 kg
	Effective stiffness	4.25×10^4 N/m

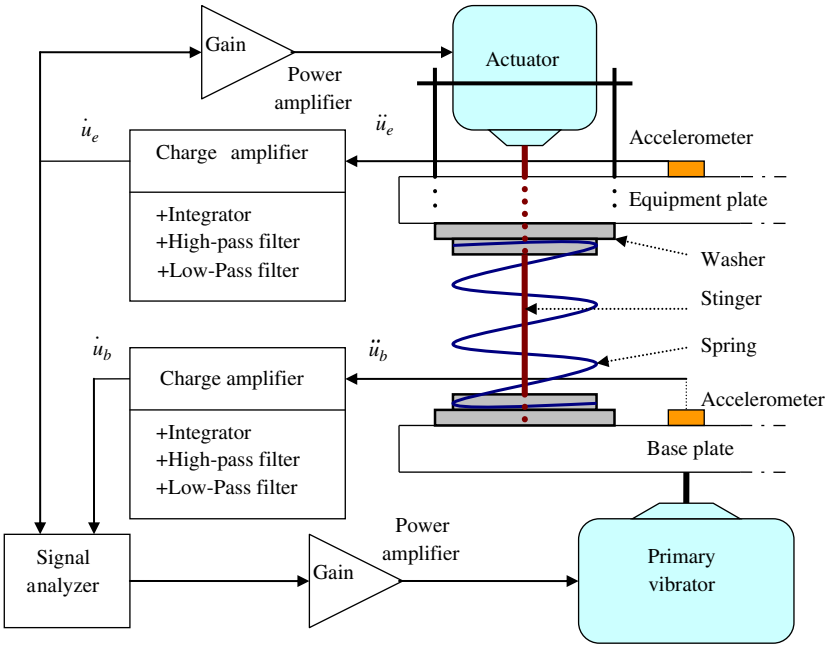

Fig. 7. Schematic diagram of one corner of the four-spring active vibration isolation system. The acceleration of the equipment and the base are given by $\ddot{u}_e$ and $\ddot{u}_b$, respectively.

the reference signal rather than the input force because the input voltage is approximately proportional to the input force within the frequency range of interest in this study [19].

The predicted and measured open-loop frequency responses are shown in Fig. 8. The first peak at 11.8 Hz is dominated by the equipment response, in which the mass of the equipment structure interacts with the serial combination of the four parallel springs and base stiffness. The second peak, at approximately 50 Hz, is dominated by the base dynamics, in which the base mass interacts on the parallel combination of the four parallel springs and base stiffness. The first resonance in the helical springs at about 404 Hz can be clearly identified and compares well with predictions. However, the second isolator resonance is strongly coupled with some flexural modes in the equipment plate, which can no longer be assumed to be rigid at these relatively high frequencies. Apart from some differences in the resonant amplitudes, the theoretical results agree fairly well with the experimental measurements, except for the unmodelled rotational modes around 32 and 289 Hz, the unmodelled flexural modal behaviour in the equipment plate around 327 Hz and in the frequency range above 500 Hz. The phase shift at low frequencies, which is $>90^\circ$, is due to the phase advances in the power amplifier and charge amplifiers. The phase shift at high frequencies, where the phase tends to decrease below -90°, is due to the phase lag in the low-pass filters incorporated inside the charge amplifiers.

The potential instability occurs at the first resonance of the helical springs as predicted. This supports the stability analysis in the theoretical study. The flexural mode in the equipment plate at 327 Hz also has the potential to destabilise the system, which is not considered in the theoretical study here but was identified by Kim et al. [10]. The cause of the instability in the experiment also includes the phase advances in the power and charge amplifiers. The power amplifier has a phase advance of up to about 90° at very low frequencies (under 5 Hz). Furthermore, an additional phase advance occurs in the charge amplifier. A phase advance of $>90^\circ$ at very low frequencies can cause the Nyquist plot of the plant response

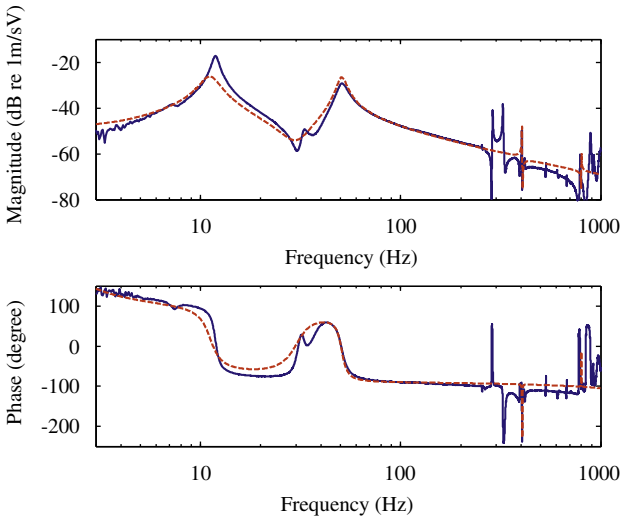

Fig. 8. Measured, solid line, and predicted, dashed line, open-loop frequency response of the four-spring active vibration isolation system.

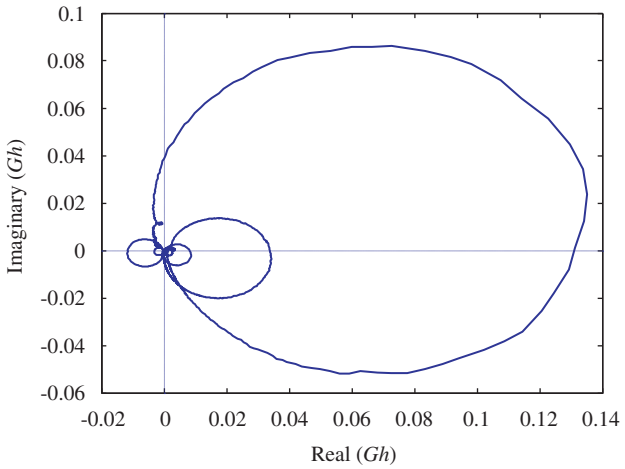

Fig. 9. Measured Nyquist plot of the open-loop frequency response of the four-spring active vibration isolation system.

to cross the negative real axis, thus making the system unstable to high gain [20]. The experimental plant can also be potentially unstable at very high frequencies due to the high-order modes in the experimental structure as well as electrical issues. The low-pass filter incorporated inside the charge amplifier produces an effective time delay in the control loop, which can make the system unstable at high frequencies. Furthermore, the phase shift in the electromagnetic actuators can also be modelled as an additional time delay [10].

Fig. 9 depicts the Nyquist plot of the open-loop frequency response corresponding to the frequency range of Fig. 8. Two loops in the left half of the complex plane crossing the negative real axis are caused by the first resonance in the helical springs at 404 Hz (smaller loop on left hand side) and the flexural mode in the equipment plate at 327 Hz (larger loop on left hand side), respectively. The Nyquist plot of the plant response also crosses the negative real axis at very low frequencies due to the phase advances in the power and charge amplifiers, which is not shown in Fig. 9. In these experiments, it was this phase shift that caused instability at very low frequencies before the potential instabilities above became important.

4.3. Control performance

A single-channel AVF control on the four-spring active vibration isolation system was implemented on each of the four springs. The primary vibrator was driven with white noise. The velocity responses of the equipment were obtained using accelerometers through charge amplifiers and then passed to the signal analyzer. The velocity response at the centre of the

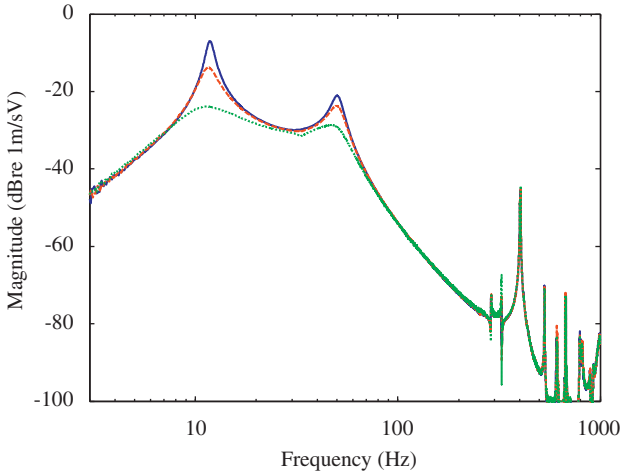

Fig. 10. Measured velocity response of the equipment plate per unit voltage to the power amplifier of the four-spring active vibration isolation system with various feedback gains: without control, solid line; low control gain, dashed line; and high control gain, dotted line.

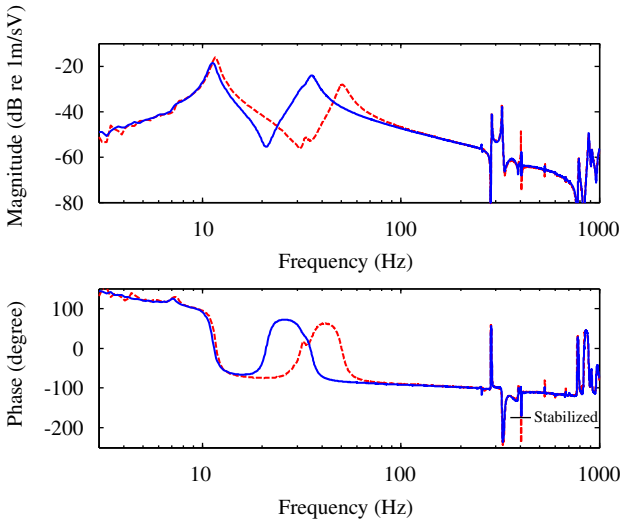

Fig. 11. Measured open-loop frequency response of the four-spring active vibration isolation system with (solid line) or without (dashed line) additional mass on the base.

equipment plate was fed back into four actuators through a power amplifier to generate the control forces, which were identical for each actuator. Each feedback channel had thus an equal, constant feedback gain.

Fig. 10 shows the measured velocity response of the equipment plate per unit voltage to the power amplifier, which drove the primary vibrator, without control and with various control gains. The equipment and base resonance peaks are attenuated with an increased control gain as predicted. However, the resonance peaks at high frequencies including the first resonance peak in the springs are not reduced, because the mass of the equipment structure dominates the response in this frequency range as discussed in the theoretical study. Closer examination of the first resonance in the helical springs at 404 Hz shows that there is a small amplification caused by the phase shift at this frequency. There is similar amplification in the amplitude occurs around 327 Hz also due to the corresponding phase shift. The gain margin for the higher feedback gain used was 1.8 dB, determined by the very low frequency instability.

4.4. Stabilisation of the AVF control system

Because the base structure is much lighter and more flexible than the equipment structure, the system is much more likely to be unstable at an isolator resonance frequency. Two approaches were implemented experimentally to stabilise the AVF control system based on the previous theoretical analysis.

As shown theoretically, adding more mass to the base structure is a simple way to change the base response. A mass of 1.8 kg was attached to the base plate to investigate its stabilising effect on the system. The measured open-loop frequency response of the improved system is shown in Fig. 11, in which the original open-loop frequency response is also shown for comparison. It can be seen that the base resonance is reduced to a lower frequency due to the attachment of the mass. The amplitude and phase of the first isolator resonance are also affected. The phase at the first isolator resonance is reduced from -235° to -175°, thus eliminating the potential instability due to this effect. However, the flexural mode in the equipment plate at 327 Hz is not affected, because the change of the base dynamics does not affect the flexural modal behaviour in the equipment plate. The control performance of the system with the additional mass on the base is shown in Fig. 12. It can be seen that the resonance peaks at low frequencies are attenuated without the compromise of an increase at the first resonance in the helical springs. The maximum gain, however, is still limited by the phase shift at very low frequency.

This AVF control system can also been stabilised by introducing a lead compensator into the feedback control loop [21]. Fig. 13 shows the open-loop frequency response of the four-spring active vibration isolation system with a first-order lead compensator, which is carefully tuned to compensate for the phase lag caused by the first isolator resonance at 404 Hz. The open-loop frequency response of the original system is also shown for comparison. It should be noted that the phase is constrained to be $< -180^\circ$ both at the first isolator resonance frequency of 404 Hz and at the flexural mode in the equipment plate of 327 Hz. These potential instabilities are thus eliminated by introducing the lead compensator.

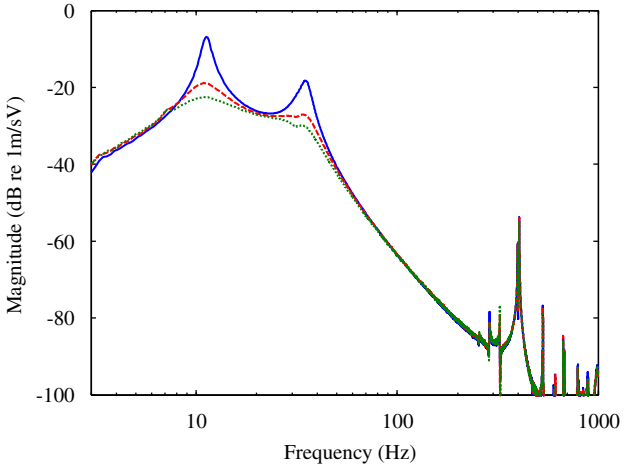

Fig. 12. Measured velocity response of the equipment plate per unit voltage to the power amplifier of the four-spring active vibration isolation system with additional mass on the base under various feedback gains: without control, solid line; low control gain, dashed line; and high control gain, dotted line.

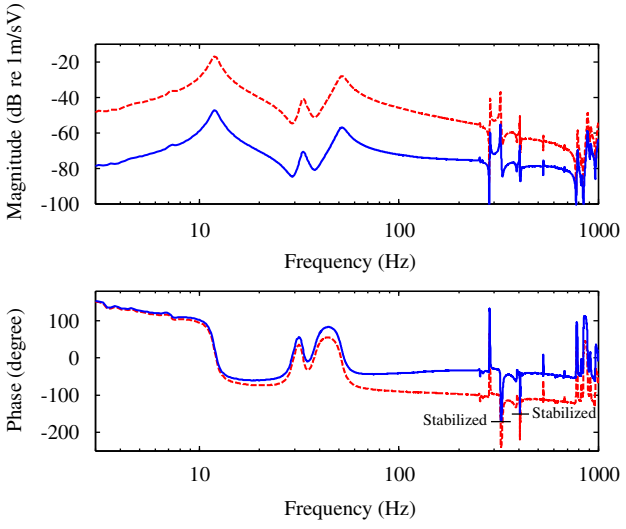

Fig. 13. Measured open-loop frequency response of the four-spring active vibration isolation system with (solid line) or without a lead compensator (dashed line).

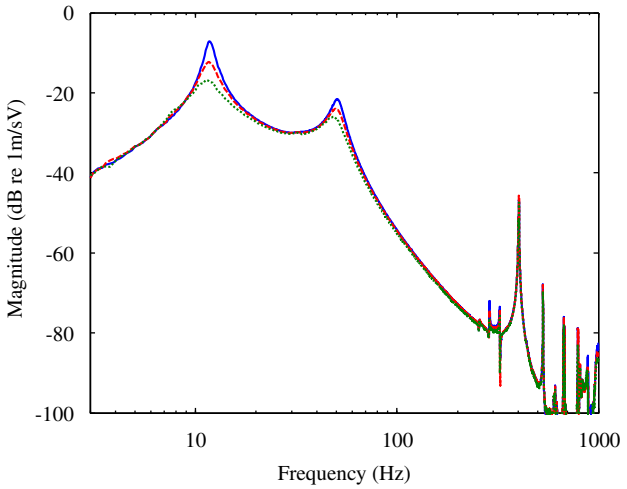

Fig. 14. Measured velocity response of the equipment plate per unit voltage to the power amplifier of the four-spring active vibration isolation system with a lead compensator under various feedback gains: without control, solid line; low control gain, dashed line; and high control gain, dotted line.

However, it should also be noted that the magnitude of the open-loop frequency response is reduced due to the lead compensator. As a consequence, the instability in such a control system does not occur at low frequencies as before. Instead, the control system became unstable at about 1160 Hz, which can be identified as a flexible mode in the base plate. The decrease in the magnitude of the open-loop frequency response also means that greater feedback control gain is required for the stabilised system with the lead compensator to achieve the same control performance as that of the original system. The control performance of the stabilised system with the lead compensator is shown in Fig. 14. It can be seen that the resonance peaks at low frequencies are attenuated without increasing both the first resonance in the helical springs and the flexural mode in the equipment plate of 327 Hz. However, the control performance is limited due to the instability occurring at the flexural mode in the base plate at approximately 1160 Hz.

5. Conclusions

In this paper, the effects of resonances in a distributed parameter isolator on the control performance and stability of an AVF control system have been investigated. The AVF control system was first studied on a system with a rigid base, and then extended to include the resonance behaviour of the base. It was shown that AVF control is only effective in attenuating the resonance peaks at relatively low frequencies, and it cannot suppress the resonance peaks in the isolator at higher frequencies where the equipment mass dominates the response. Although the AVF control system for a base excited system was shown to be unconditionally stable it has a potential to become unstable if the base dynamics are considered. A stability condition in terms of the overall system mode shapes evaluated at the equipment and base has been proposed. The theoretical findings have been validated by experiments on a four-spring active vibration isolation system which was configured to act as a one-dimensional system. Two approaches, adding more mass to the base and introducing a lead compensator into the control loop, have been shown to be effective in stabilizing the AVF control system.

References

[1] C.E. Crede, J.E. Ruzicka, Theory of vibration isolation, in: C.M. Harris, A.G. Piersol (Eds.), *Shock and Vibration Handbook*, McGraw-Hill, New York, 2002.
[2] D.J. Mead, *Passive Vibration Control*, Wiley, Chichester, 1999.
[3] M.J. Brennan, N.S. Ferguson, Vibration control, in: F.J. Fahy, J.G. Walker (Eds.), *Advanced Applications in Acoustics, Noise and Vibration*, E&FN SPON, London, 2004.
[4] M. Serrand, S.J. Elliott, Multichannel feedback control for the isolation of base-excited vibration, *Journal of Sound and Vibration* 234 (2000) 681–704.
[5] S.S. Rao, *Mechanical Vibrations*, Addison-Wesley, Reading, Massachusetts, 1984.
[6] D.C. Karnopp, Active and semi-active vibration isolation, *Transactions of the American Society of Mechanical Engineers, Journal of Mechanical Design* 177 (1995) 177–185.
[7] M.J. Brennan, S.J. Elliott, X. Huang, A demonstration of active vibration isolation using decentralised velocity feedback control, *Smart Materials and Structures* 14 (2006) N1–N4.
[8] C.R. Fuller, S.J. Elliott, P.A. Nelson, *Active Control of Vibration*, Academic Press, New York, 1996.
[9] M.J. Balas, Direct velocity feedback control of large space structures, *Journal of Guidance and Control* 2 (1979) 252–253.
[10] S.M. Kim, S.J. Elliott, M.J. Brennan, Decentralized control for multichannel active vibration isolation, *IEEE Transactions on Control Systems Technology* 9 (2001) 93–100.
[11] X. Huang, S.J. Elliott, M.J. Brennan, Active isolation of a flexible structure from base vibration, *Journal of Sound and Vibration* 263 (2003) 357–376.
[12] S.M. Joshi, Robustness properties of collocated controllers for flexible spacecraft, *Journal of Guidance and Control* 9 (1986) 85–91.

[13] S.J. Elliott, L. Benassi, M.J. Brennan, P. Gardonio, X. Huang, Mobility analysis of active isolation systems, *Journal of Sound and Vibration* 271 (2004) 297–321.
[14] E.E. Ungar, C.W. Dietrich, High-frequency vibration isolation, *Journal of Sound and Vibration* 4 (1966) 224–241.
[15] M. Harrison, A.O. Sykes, M. Martin, Wave effects in isolation mounts, *Journal of the Acoustical Society of America* 24 (1952) 62–71.
[16] J.C. Snowdon, Vibration isolation: use and characterization, *Journal of the Acoustical Society of America* 66 (1979) 1245–1274.
[17] P. Gardonio, M.J. Brennan, Mobility and impedance methods in structural dynamics, in: F.J. Fahy, J.G. Walker (Eds.), *Advanced Applications in Acoustics, Noise and Vibration*, E&FN SPON, London, 2004.
[18] B. Yan, M.J. Brennan, S.J. Elliott, N.S. Ferguson, The effects of internal resonances in vibration isolators under absolute velocity feedback control, *Proceedings of the 19th International Congress on Acoustics*, Madrid, Spain, 2007, Paper SAV-03-009, CD-ROM.
[19] M.Z. Ren, K. Seto, F. Doi, Feedback structural-borne sound control of a flexible plate with an electromagnetic actuator: the phase lag problem, *Journal of Sound and Vibration* 205 (1997) 57–80.
[20] M.J. Brennan, K.A. Ananthaganeshan, S.J. Elliott, Instabilities due to instrumentation phase-lead and phase-lag in the feedback control of a simple vibrating system, *Journal of Sound and Vibration* 304 (2007) 466–478.
[21] G.F. Franklin, J.D. Powell, A. Emami-Naeini, *Feedback Control of Dynamic Systems*, fourth ed., Prentice-Hall, New Jersey, 2002.